A&A 601, A50 (2017)
DOI: 10.1051/0004-6361/201628551

Astronomy & Astrophysics

Submillimeter spectra of 2-hydroxyacetonitrile (glycolonitrile; $HOCH_2CN$) and its searches in GBT PRIMOS observations of Sgr B2(N)⋆

L. Margulès[1], B. A. McGuire[2], M. L. Senent[3], R. A. Motiyenko[1], A. Remijan[2], and J. C. Guillemin[4]

[1] Laboratoire de Physique des Lasers, Atomes, et Molécules, UMR CNRS 8523, Université de Lille I, 59655 Villeneuve d'Ascq Cedex, France
e-mail: laurent.margules@univ-lille1.fr
[2] National Radio Astronomy Observatory, Charlottesville, VA 22903, USA
[3] Departamento de Química y Física Teóricas, Instituto de Estructura de la Materia, IEM-C.S.I.C., Serrano 121, 28006 Madrid, Spain
[4] Institut des Sciences Chimiques de Rennes, École Nationale Supérieure de Chimie de Rennes, CNRS, UMR 6226, 11 allée de Beaulieu, CS 50837, 35708 Rennes Cedex 7, France

Received 18 March 2016 / Accepted 10 October 2016

ABSTRACT

Context. Recent experimental works have studied the possible formation of hydroxyacetonitrile on astrophysical grains. It was formed from hydrogen cyanide (HCN) and formaldehyde (H_2CO) in the presence of water under interstellar medium conditions. Because these precursor molecules are abundant, hydroxyacetonitrile is an excellent target for interstellar detection.
Aims. Previous studies of the rotational spectra were limited to 40 GHz, resulting in an inaccurate line list when predicted up to the millimeter-wave range. We measured and analyzed its spectra up to 600 GHz to enable is searches using cutting-edge millimeter and submillimeter observatories.
Methods. The molecule 2-hydroxyacetonitrile exhibits large amplitude motion that is due to the torsion of the hydroxyl group. The analysis of the spectra was made using the RAS formalism available in the SPFIT program with Watson's S-reduction Hamiltonians.
Results. The submillimeter spectra of hydroxyacetonitrile, an astrophysically interesting molecule, were analyzed. More than 5000 lines were fitted with quantum number values reaching 75 and 25 for J and K_a, respectively. An accurate line list and partition function were provided. A search for hydroxyacetonitrile in publicly available GBT PRIMOS project, IRAM 30 m, and *Herschel* HEXOS observations of the Sgr B2(N) high-mass star-forming region resulted in a non-detection; upper limits to the column density were determined.

Key words. ISM: molecules – methods: laboratory: molecular – submillimeter: ISM – molecular data – line: identification

1. Introduction

More than 30 nitriles (organic cyanides) have been observed to date in the interstellar medium (ISM). Among these are the well-known family of cyanopolyynes, and isopropyl cyanide, the first branched hydrocarbon detected in the ISM (Belloche et al. 2014). This large dataset is useful in constraining models of nitrile formation in the ISM, and in predicting which other nitrile species might be present and detectable. However, many simple nitriles have yet to be detected. These non-detections could be due to a weak or null dipolar moment (for example cyanogen NCCN or 2-butyne-1,4-dinitrile NC–C≡C–CN) or to the lack of recorded microwave spectra caused by unknown or difficult syntheses of the target products. With the advent of state-of-the-art millimeter and submillimeter facilities like the Stratospheric Observatory for Infrared Astronomy (SOFIA) and the Atacama Large Millimeter/submillimeter Array (ALMA), laboratory studies of rotational spectra in this frequency range are critical for advancing the field. Such work will have to be followed by attempts, both in the laboratory and through theoretical models, to understand formation processes and observed interstellar abundances (or upper limits).

The simplest cyanohydrine, 2-hydroxyacetonitrile (glycolonitrile; $HOCH_2CN$), is readily formed in the lab by the addition of hydrogen cyanide (HCN) to formaldehyde (H_2CO) in water (Gaudry 1955). It is thought to play an important role in prebiotic chemistry, and could lead to the formation of a number of simpler organic molecules (Arrhenius et al. 1994). The formation of 2-hydroxyacetonitrile in astrophysical ices was first studied from a theoretical point of view (Woon 2001). Recently, its formation and photolytic decomposition on interstellar grains have been experimentally evaluated. These studies show that under these conditions, HCN reacts with H_2CO in the presence of H_2O to form $HOCH_2CN$ (Danger et al. 2012, 2014). Although not studied, the hydrogen-atom bombardment of formyl cyanide (HC(=O)CN) could also lead to the formation of $HOCH_2CN$, as could do the reaction of CN or OH with H_2COH or CH_2CN, respectively. Photochemistry of pure $HOCH_2CN$ leads to the formation of HC(=O)CN, HCN, ketenimine (H_2C=C=NH), H_2CO, CO, and CO_2 (Danger et al. 2013). It should be noted that most of the compounds cited as possible precursors or as photoproducts have been detected in the ISM.

⋆ Hydroxyacetonitrile fit is only available at the CDS via anonymous ftp to cdsarc.u-strasbg.fr (130.79.128.5) or via http://cdsarc.u-strasbg.fr/viz-bin/qcat?J/A+A/601/A50

The gas-phase, infrared spectrum of $HOCH_2CN$ has been recently reinvestigated (Chrostowska et al. 2015), while the microwave spectrum of $HOCH_2CN$ has not been treated since it was first observed by Cazzoli et al. (1973) from 8–40 GHz. The gauche rotamer has been observed. Doublets of the rotational transitions were observed arising from tunneling between the two equivalent gauche rotamers. The rotational constants indicate that the angle between the HOC and OCC planes at the potential minima is approximately 123° from the *trans* position, while the rotational constants calculated from a molecular model, and the potential functions, indicate that this angle is likely closer to 116°.

New spectra were measured in Lille in the range 150–600 GHz, and combined with high-level ab initio calculations for an accurate analysis. A search of the publicly available GBT PRIMOS project, IRAM 30 m, and *Herschel* HEXOS observations of Sgr B2(N) for the molecule found no evidence for a cold population of the species, and upper limits were established.

2. Experiments

2.1. Synthesis

$HOCH_2CN$ has been prepared as previously reported (Gaudry 1947, 1955).

2.2. Lille – submillimeter spectra

The measurements from 50–660 GHz were performed using the Lille spectrometer (Zakharenko et al. 2015). A quasi-optic dielectric hollow waveguide, 3 m in length, containing $HOCH_2CN$ was used as the sample cell in the spectrometer. The measurements were typically performed at pressures of 10 Pa and at room temperature. The frequency ranges of 50–315 and 400–550 GHz were covered with various active and passive frequency multipliers where an Agilent synthesizer (12.5–18.25 GHz) was used as the source of radiation. Estimated uncertainties for measured line frequencies are 30 kHz and 50 kHz depending on the observed signal-to-noise ratio and the frequency range.

3. Theoretical calculations

High-level ab initio calculations were used to determine the geometries of the two conformers, *gauche* and *trans*, and to compute low-energy torsional levels. Electronic structure calculations were performed using both the MOLPRO (Werner et al. 2012) and GAUSSIAN packages (Frisch et al. 2009). The torsional energy levels were determined by variational calculations using the procedure previously employed for other non-rigid species (Senent 2004).

The equilibrium structures, *gauche* and *trans*, of $HOCH_2CN$, as well as the most relevant spectroscopic parameters (equilibrium rotational constants and the one-dimensional potential energy surface, 1D-PES, for the hydroxyl torsion) were computed using explicitly correlated coupled cluster theory with single and double substitutions augmented by a perturbative treatment of triple excitations (CCSD(T)-F12b) (Knizia et al. 2009; Werner et al. 2007) with an aug-cc-pVTZ basis set (Kendall et al. 1992). Second-order Möller-Plesset theory (MP2) was employed to determine vibrational corrections for the potential energy surface and the α_j^r vibration-rotation constants. For the explicitly correlated calculations, the MOLPRO default options were selected.

Table 1. Calculated ground-state rotational constants (MHz), energies and conformational barriers (cm^{-1}), and dipole moments (Debye) for $HOCH_2CN$.

Parameter	*gauche*–$HOCH_2CN$	*trans*–$HOCH_2CN$
A_0	33 621.46	35 519.53
B_0	4828.88	4833.28
C_0	4370.77	4369.98
ΔE	506.3	
V(*gauche-gauche*)	425.8	
V(*gauche-trans*)	645.4	
μ	2.94	
μ_a	2.32	
μ_b	1.31	
μ_c	1.23	

The ground vibrational state rotational constants of the two conformers were determined from the equilibrium parameters using Eq. (1) (cf. Senent et al. 2015)

$$B_0 = B_e + \Delta B_e^{core} + \Delta B_{vib}, \quad (1)$$

where ΔB_e^{core} represents the core-valence correlation correction and ΔB_{vib} is the vibrational contribution to the rotational constants derived from the vibration-rotation interaction parameters. The results are shown in Table 1.

The low torsional energy levels were calculated using a variational solution to the Hamiltonian given in Eq. (2) (Senent 1998a,b):

$$\hat{H}(\alpha) = -\left(\frac{\partial}{\partial\alpha}\right) B_\alpha \left(\frac{\partial}{\partial\alpha}\right) + V^{eff}(\alpha). \quad (2)$$

Here, α is the OH torsional coordinate, B_α are the kinetic energy parameters, and $V^{eff}(\alpha)$ is the vibrationally corrected 1D-PES (Császár et al. 2004) shown in Fig. 1.

The ground vibrational state splits into two components E(0^-) and E(0^+) because of tunneling in the V(*gauche-gauche*) barrier. Ab initio calculations predict a splitting of 96 563.148 MHz (3.2210 cm^{-1}). In addition, the first excited vibrational state shows two components lying at 223.05 cm^{-1} (1^+) and 261.27 cm^{-1} (1^-) over the ground state. The first *trans* level lies at 459 cm^{-1} (0).

4. Analysis of the spectra

We have analysed the spectra of the *gauche* conformer, which is the more stable of the two. This analysis was not trivial because the gauche rotamer exhibits one large amplitude motion (LAM) with a symmetric two minima potential due to the two equivalent gauche rotamers. As a result of tunneling through the barrier to OH-group torsion, the ground state is split into two substates: 0^- and 0^+. This rotamer is very close to a symmetric prolate rotor with an asymmetry parameter $\kappa = -0.968$. Like other nitriles, the dipole moment is large; the values we determined from MP2/aug-cc-pVTZ ab initio calculations and are given in Table 1. The component along the *c*-axis of the dipole moment is linked to torsional motion, giving rise to transitions between the two torsional substates 0^- and 0^+.

An initial prediction of the spectra was made for the two substates 0^- and 0^+ separately with Watson's Hamiltonian in the I^r representation using the rotational parameters from

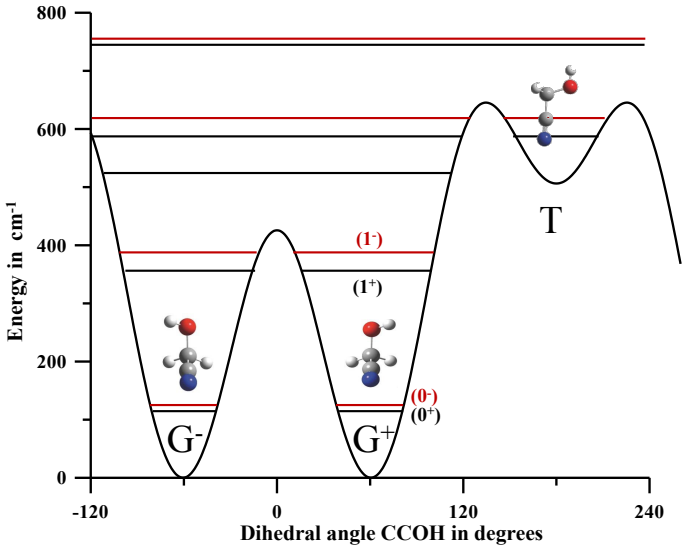

Fig. 1. CCSD(T)-F12 potential energy as a function of the hydroxyl group internal rotation coordinate.

Cazzoli et al. (1973) and the quartic centrifugal distortion constants obtained from the harmonic force field at the MP2/aug-cc-pVTZ level of theory. We first assign the *A*-type, *R*-branch transitions, which are the brightest in our spectra. Owing to the rather strong interaction between these two sublevels, it was not possible to assign and fit data even for $K_a = 0$ and 1 transitions in the lower range of the spectra 150–315 GHz. Some less perturbed levels were found above 400 GHz, and an assignment and fit was possible by treating the two sublevels separately for K_a values up to 2 in the 400–500 GHz range, improving the values of the rotational and the centrifugal distortion constants. The two sublevels were then merged in a unique fit, using the energy difference between the 0^- and 0^+ levels determined by Cazzoli et al. (1973) as the starting point. We note that this value, 110 700 MHz, is close to the one we determined, 112 672.5526(30) MHz.

For the global fit, a model based on the reduced axis system (RAS) approach proposed by Pickett (1972) was implemented in the widely used SPFIT/SPCAT programs for fitting and predicting molecular spectra. We have successfully employed this method in previous studies showing the same kind of double minimum LAM (Motiyenko et al. 2010, 2015; Smirnov et al. 2013). Is has been shown by Christen et al. (2002) that the RAS formalism is equivalent to the IAM approches developed by Hougen and coworkers for molecules with several large amplitude motions (Hougen 1985; Coudert & Hougen 1988).

The perturbation terms in the RAS Hamiltonian are equivalent in this case to off-diagonal Coriolis coupling terms; the Hamiltonian used has the form given in Eq. (3):

$$H = H_{\mathrm{R}} + H_{\mathrm{C}}. \tag{3}$$

More details about the exact expression of the Hamiltonian can be found in Christen & Müller (2003). In that work, they also proposed the use of average rotational constants for both substates introducing a Hamiltonian for centrifugal distortion corrections, given in Eq. (4),

$$H_{\mathrm{R}} = H_{\mathrm{S}} + H_{\Delta}, \tag{4}$$

where H_{R} is the standard Watson S-reduction Hamiltonian in the I^r coordinate representation and H_{Δ} defined in Eq. (5),

$$H_{\Delta} = E^* + E^*_J J^2 + E^*_K J^2_z + E^*_2(J^2_+ + J^2_-) + \dots, \tag{5}$$

where E^* is a half energy difference between two *A* or *B* levels ($\Delta E = 2E^*$), and J, J_z, and $J_\pm = J_x \pm iJ_y$ are the rotational angular momentum operator and its components. This procedure has two main advantages. First, a unique set of rotational and centrifugal distortion parameters permits an easier comparison with ab initio calculations. Second, this method is more robust and avoids correlations between different rotational and Coriolis coupling parameters.

Including the F_{2ac} parameter slightly decreases the standard deviation of fit from 29.2 kHz (wrms: 0.931) to 28.5 kHz (wrms: 0.907), and it seems to be determined: −0.0967(82). Looking closely, however, including F_{2ac} has several negative consequences on the fit. Ten lines were rejected from the fit after including F_{2ac}. We also notice a strong influence on F_{acK}: its values change from 0.009943(25) to 0.00304(59) when fitting F_{2ac}. This influence is confirmed by looking at the correlation coefficient; there is almost full correlation with F_{ac}, F_{acJ}, and F_{acK}, with coefficients of −0.996, −0.990, and 0.999, respectively. We have thus decided to keep F_{2ac} fixed to zero in the final fit. The final set of parameters obtained are in Table 2. In total, 5128 distinct lines were assigned with maximum values for J and K_a of 75 and 25, respectively. Part of the new measurements are in Table 3. Owing to its large size, the complete version of the global fit Table (S1) is supplied at the CDS[1]. The fitting files .lin (S2), .par (S3), and the prediction .cat (S4) are also available at CDS.

5. Observations

We have conducted a search of the publicly available Prebiotic Interstellar Molecular Survey (PRIMOS) project observations of the high-mass star-forming region Sgr B2(N) for a signal from $HOCH_2CN$. PRIMOS is a near-frequency continuous, 1–50 GHz broadband molecular line survey conducted with the *Robert C. Byrd* Green Bank Telescope (GBT), and centered on the Large Molecular Heimat at (J2000) $\alpha = 17^{\mathrm{h}}47^{\mathrm{m}}19\overset{\mathrm{s}}{.}8$, $\delta = -28°22'17''$. Full observational and data-reduction details are given in Neill et al. (2012); the entire dataset is accessible online[2]. The PRIMOS observations vary in RMS noise level from ∼3–8 mK across the band; however, we find no evidence for emission or absorption from $HOCH_2CN$ in the survey. Below, we establish upper limits to the column density for a variety of physical conditions, and briefly discuss the possibilities for future searches for this molecule.

We follow the convention of Hollis et al. (2004) using Eq. (6) to calculate an upper limit to column density N_T, given a rotational partition function Q, upper state energy E_{U}, rotational temperature T_{r}, transition frequency ν, intrinsic line strength $S\mu^2$, observed intensity ΔT^*_{A}, linewidth ΔV, telescope efficiency η_{B}, and background temperature T_{bg}:

$$N_T = \frac{Q\mathrm{e}^{E_{\mathrm{u}}/kT_{\mathrm{r}}}}{\frac{8\pi^3}{3k}\nu S\mu^2} \times \frac{\frac{1}{2}\sqrt{\frac{\pi}{\ln(2)}}\frac{\Delta T^*_{\mathrm{A}}\Delta V}{\eta_{\mathrm{B}}}}{1-\frac{\mathrm{e}^{h\nu/kT_{\mathrm{r}}}-1}{\mathrm{e}^{h\nu/kT_{\mathrm{bg}}}-1}}. \tag{6}$$

The structure of Sgr B2(N) is complex, with a compact (∼5″) hot molecular core surrounded by a more extended, colder molecular shell (Hollis et al. 2007). The background continuum structure against which molecules in this shell absorb is ∼20″ in diameter (see, e.g., Fig. 3*b* of Mehringer et al. 1993). For the purposes of this study, we assume these same source sizes for warm molecular material and cold molecular material and explicitly calculate

[1] http://cdsweb.u-strasbg.fr/A+A.htx
[2] www.cv.nrao.edu/PRIMOS

Table 2. Spectroscopic parameters of the *gauche* conformer of 2-hydroxyacetonitrile.

Parameters in MHz	This work	Cazzoli et al.[a]	Theory[b]
	Rotational and centrifugal distortion constants		
A	33 609.53194(27)[c]	0^-: 33 605.57(22)	33 621.46
		0^+: 33 611.68(22)	
B	4838.014347(41)	0^-: 4840.44(4)	4828.88
		0^+: 4835.51(4)	
C	4377.304462(40)	0^-: 4377.60(3)	4370.77
		0^+: 4376.44(3)	
$D_J * 10^3$	3.093051(44)	2.7 (0.8)	3.079
$D_{JK} * 10^3$	−63.89803(34)	−81 (5)	−65.329
$D_K * 10^3$	969.2208(61)		958.548
$d_1 * 10^3$	−0.695725(10)		−0.68705
$d_2 * 10^3$	−0.041757(18)		−0.03659
$H_J * 10^6$	0.0107392(81)		
$H_{JK} * 10^6$	−0.16090(71)		
$H_{KJ} * 10^6$	−3.6005(17)		
$H_K * 10^6$	82.883(56)		
$h_1 * 10^6$	0.0044035(40)		
$h_2 * 10^6$	0.0005288(27)		
$h_3 * 10^6$	0.00007335(95)		
$L_K * 10^9$	−3.14(17)		
$L_{KKJ} * 10^9$	0.3292(25)		
$L_{JK} * 10^9$	−0.04864(29)		
$L_{JJK} * 10^9$	0.001496(12)		
$L_J * 10^9$	−0.00005190(75)		
$l_1 * 10^9$	−0.00002619(46)		
$l_2 * 10^9$	−0.00000544(39)		
$l_3 * 10^9$	−0.00000236(17)		
	Tunneling splitting constants		
E	112 672.5526(30)	110 700 fixed	96563.148[d]
E_J	1.0954348(39)		
E_K	−13.606157(53)		
$E_{JJ} * 10^3$	−0.00749(11)		
$E_{JK} * 10^3$	−0.19132(72)		
$E_{KK} * 10^3$	0.44739(78)		
E_2	0.331606(22)		
$E_{2J} * 10^3$	−0.0073918(30)		
$E_{2K} * 10^3$	1.339(22)		
$E_{2JJ} * 10^9$	0.07826(71)		
$E_{2JK} * 10^9$	−21.80(20)		
$E_4 * 10^6$	−5.215(60)		
$E_{4J} * 10^9$	0.1756(13)		
	Coriolis coupling constants		
F_{bc}	−5.7926(14)		
$F_{bcK} * 10^3$	43.41(74)		
$F_{bcJ} * 10^3$	−0.113411(86)		
$F_{bcKK} * 10^6$	−19.08(43)		
$F_{bcJK} * 10^6$	0.4789(72)		
$F_{2bc} * 10^6$	86.5(14)		
F_{ac}	75.52596(18)		
$F_{acJ} * 10^3$	−0.05771(28)		
$F_{acK} * 10^3$	9.943(25)		
$F_{acJK} * 10^6$	0.485(16)		
$F_{acKK} * 10^6$	−9.229(30)		
Number of distinct lines			5128
Number of parameters			47
$J''_{\max}, K''_{a,\max}$			75, 25
Standard deviation of the fit (in kHz)			29.2
Weighted deviation of fit			0.931

Notes. [(a)] Cazzoli et al. (1973). [(b)] Calculated using CCSD(T)-F12 theory and the MP2/aug-cc-pVTZ anharmonic force field. [(c)] Number in parentheses is one standard deviation in unit of the last digit. [(d)] Calculated by solving variationally the Hamiltonian, see text for details.

Table 3. Measured frequencies of the *gauche* conformer of 2-hydroxyacetonitrile and residuals from the fit (full fit is available at the CDS: S1).

Upper level				Lower level				Frequency(Unc.)	o.-c.
J''	K_a''	K_c''	$v_t''^a$	J'	K_a'	K_c'	$v_t'^a$	(in MHz)	(in MHz)
75	0	75	1	74	1	74	1	657 112.073(0.030)	−0.0230
75	1	75	1	74	0	74	1	657 112.073(0.030)	−0.0230
18	9	9	1	17	8	10	1	657 168.387(0.030)	0.041
18	9	10	1	17	8	9	1	657 168.387(0.030)	0.041
44	10	35	1	44	9	35	0	657 260.517(0.030)	0.002
43	10	34	1	43	9	34	0	657 600.923(0.030)	0.027
12	8	4	1	11	7	4	0	658 010.623(0.030)	0.035
12	8	5	1	11	7	5	0	658 010.623(0.030)	0.035
36	10	27	1	36	9	27	0	659 576.402(0.030)	0.057
28	14	15	0	28	13	15	1	659 608.388(0.030)	−0.059
35	10	26	1	35	9	26	0	659 806.414(0.030)	0.017
25	6	19	1	24	5	19	0	659 980.141(0.030)	−0.022

Notes. [(a)] Following SPFIT format the torsional substate 0^- and 0^+ are labeled 0 and 1, respectively.

the spatial overlap of these regions with the GBT beam as its size varies across the frequency coverage.

Hollis et al. (2007) establish the background continuum temperature at 85 points across the PRIMOS frequency coverage. These continuum measurements range from more than 100 K at low frequencies to just above the CMB at the higher frequencies, although these measurements are not corrected for any assumed source geometry or beam dilution effects. The authors attribute this to non-thermal continuum in the source. We adopt their measurements of the continuum for these calculations, but correct them for the overlap of the assumed source size of the continuum-emitting region with the GBT beam in the PRIMOS observations.

The tabulated values for the partition function are given in Table 4, with $Q_{\rm tot}(T) = Q_{\rm vib}(T)Q_{\rm rot}(T)$. The rotational partition function is calculated at each temperature by direct state counting according to Eq. (7) (Gordy & Cook 1984):

$$Q_r = \frac{1}{\sigma}\sum_{J=0}^{J=\infty}\sum_{K=-J}^{K=J}(2J+1)\mathrm{e}^{-E_{J,K}/kT_{\rm ex}}. \quad (7)$$

The vibrational partition function was calculated with respect to the zero-point level using the expression:

$$Q(T)_{\rm vib} = \prod_{i=1}^{3N-6}\frac{1}{1-\mathrm{e}^{-E_i/kT}}. \quad (8)$$

The four lowest vibrational excited states levels were considered. The remaining ones above 885 cm^{-1} were found to have no influence on the partition function calculations. Their frequencies are respectively 228 cm^{-1} (328 K), 246 cm^{-1} (354 K), 343 cm^{-1} (494 K), and 576 cm^{-1} (829 K); these values were taken from Chrostowska et al. (2015).

Finally, we assume that the excitation of all $HOCH_2CN$ can be described by a single rotational temperature. We do not, however, make the assumption that this temperature is described by local thermodynamic equilibrium (LTE), meaning that the excitation temperature is not thermalized to the kinetic temperature of the gas. This approach has previously proven to be successful in modeling both the emission and absorption of molecules in PRIMOS observations (Hollis et al. 2004; Loomis et al. 2013; McGuire et al. 2016). We note, however, that several other molecules exhibit populations which cannot be described by a single excitation temperature (McGuire et al. 2012; Faure et al. 2014), and thus care should be taken to examine any single-excitation temperature results on a case-by-case basis.

In addition to the PRIMOS observations, we have also examined publicly available surveys of Sgr B2(N) from Belloche et al. (2013) [IRAM 30 m: 80–116 GHz] and Neill et al. (2014) [*Herschel* HEXOS: 480–600 GHz]. No compelling evidence for $HOCH_2CN$ is found in either survey. With the exception of the warm (200 K), extended (200″) population, the upper limits established by the PRIMOS data are not changed by more than ∼10% due to greater noise in the higher-frequency data, compared to PRIMOS.

Table 5 shows the upper limits calculated here for several different common populations of species. The given values represent the best limits achievable across all three datasets. It is immediately clear that the PRIMOS observations are most sensitive to cold populations of $HOCH_2CN$, with the established upper limits several orders of magnitude lower than for warmer excitation conditions. This occurs because for relatively large, complex species such as $HOCH_2CN$, which have large partition functions, any significant level of excitation pushes the Boltzmann peak into the mm and sub-mm regimes, resulting in low spectral intensities in the region of PRIMOS coverage. Our searches at higher frequencies suffered greatly from more heavily line-confusion-limited spectra; ALMA observations of the region are likely the only method for spatially filtering this confusion.

The first detection of methyl isocyanate (CH_3NCO), a structural isomer of $HOCH_2CN$, has recently been reported in Sgr B2(N) by Halfen et al. (2015) in a cold, extended population ($T_{\rm r}$ ∼ 26 K, N_T ∼ 2 × 10^{13} cm^{-2}) in two velocity components. A second warmer population ($T_{\rm r}$ ∼ 200 K, N_T ∼ 4 × 10^{17} cm^{-2}) was subsequently identified by Cernicharo et al. (2016) in two velocity components. For comparison, we have calculated upper limits for $HOCH_2CN$ under these excitation conditions, as well.

For the warm population of Cernicharo et al. (2016), the CH_3NCO:$HOCH_2CN$ ratio is >1000:1. The ratio for the colder population of Halfen et al. (2015) is, conversely, >1:1. If the same formation pathways are in effect for both the warm and cold populations, the upper limit established for the cold

Table 4. Rotational and vibrational partition functions at various temperatures.

T (K)	$Q(T)_{\rm rot}$	$Q(T)_{\rm vib}$
300	65 208.5016	2.8710
225	42 282.4022	1.8981
150	22 866.7336	1.2971
75	7939.2463	1.0233
37.5	2713.8889	1.0002
18.75	901.1494	1.0000
9.375	285.4325	1.0000

Table 5. Upper limits to $HOCH_2CN$ column density in PRIMOS, IRAM, and *Herschel* HEXOS observations toward Sgr B2(N) for several common conditions.

$T_{\rm r}$ (K)	Source size ($''$)	Upper limit column density (cm^{-2})
8	20	8×10^{12}
18	20	8×10^{13}
26[b]	200[b]	2×10^{13}
80	5	2×10^{15}
130	5	4×10^{15}
200	5	8×10^{15}
200[b]	200[b]	7×10^{14}

Notes. [(a)] We estimate the uncertainties in the upper limits to be ~30%, largely arising from absolute flux calibration and pointing uncertainties. [(b)] Values were chosen for comparison to CH_3NCO detection from Halfen et al. (2015) and Cernicharo et al. (2016). A source size of 200$''$ follows the assumption that the source completely fills the beam.

population is likely closer to ~10^{10} cm^{-2}. In this case, the best-case scenario for detection is likely through masing action in low-frequency transitions. Such emission enhancement has been seen in this source (Faure et al. 2014), and has indeed been used to detect extremely low-abundance species (e.g., carbodiimide, HNCNH; McGuire et al. 2012).

6. Conclusion

The spectra of 2-hydroxyacetonitrile, a molecule expected to have a role in prebiotic chemistry, were measured and analyzed up to 600 GHz. The assignment of the spectra was not obvious owing to large amplitude motion of the OH group, but was aided by high-level ab initio calculations. With the newly constrained constants, the fit and predictions are now accurate throughout the millimeter and submillimeter regions. These results enabled its search in the GBT PRIMOS survey toward Sgr B2(N). No cold population was detectable; however, the possibility of a warmer population remains, and upper limits were established.

Acknowledgements. This work was supported by the Programme National "Physique et Chimie du Milieu Interstellaire" and the Centre National d'Études Spatiales (CNES). This work was also done under ANR-13-BS05-0008-02 IMOLABS. B.A.M. is a Jansky Fellow of the National Radio Astronomy Observatory. The National Radio Astronomy Observatory is a facility of the National Science Foundation operated under cooperative agreement by Associated Universities, Inc.

References

Arrhenius, T., Arrhenius, G., & Paplawsky, W. 1994, Origins of life and evolution of the biosphere, 24, 1
Belloche, A., Garrod, R. T., Müller, H. S. P., & Menten, K. M. 2014, Science, 345, 1584
Cazzoli, G., Lister, D. G., & Mirri, A. M. 1973, J. Chem. Soc., Faraday Trans. 2, 69, 569
Christen, D., & Müller, H. S. P. 2003, Phys. Chem. Chem. Phys., 5, 3600
Christen, D., Müller, H. S. P., & Coudert, L. H. 2002, 57th International Symposium on Molecular Spectroscopy, TB03
Chrostowska, A., Darrigan, C., Dargelos, A., Benidar, A., & Guillemin, J.-C. 2015, Chem. Phys. Chem., 16, 3660
Coudert, L. H., & Hougen, J. T. 1988, J. Mol. Spectr., 130, 86
Császár, A. G., Szalay, V., & Senent, M. L. 2004, J. Chem. Phys., 120, 1203
Danger, G., Duvernay, F., Theulé, P., Borget, F., & Chiavassa, T. 2012, ApJ, 756, 11
Danger, G., Duvernay, F., Theulé, P., et al. 2013, A&A, 549, A7
Danger, G., Rimola, A., Abou Mrad, N., et al. 2014, Phys. Chem. Chem. Phys., 16, 3360
Faure, A., Remijan, A. J., Szalewicz, K., & Wiesenfeld, L. 2014, ApJ, 783, 72
Frisch, M., Trucks, G., Schlegel, H., et al. 2009, Gaussian software, version 09, revision D01
Gaudry, R. 1947, Organic Syntheses, 27, 41
Gaudry, R. 1955, Organic Syntheses, Coll, 3, 436
Gordy, W., & Cook, R. L. 1984, Microwave molecular spectra, 3rd edn. (New York: Wiley)
Hollis, J., Jewell, P., Remijan, A. J., & Lovas, F. 2007, ApJ, 660, L125
Hollis, J. M., Jewell, P., Lovas, F., & Remijan, A. 2004, ApJ, 613, L45
Hougen, J. T. 1985, J. Mol. Spectr., 114, 395
Kendall, R. A., Dunning Jr, T. H., & Harrison, R. J. 1992, J. Chem. Phys., 96, 6796
Knizia, G., Adler, T. B., & Werner, H.-J. 2009, J. Chem. Phys., 130, 054104
Loomis, R. A., Zaleski, D. P., Steber, A. L., et al. 2013, ApJ, 765, L9
McGuire, B. A., Loomis, R. A., Charness, C. M., et al. 2012, ApJ, 758, L33
McGuire, B. A., Carroll, P. B., Loomis, R. A., et al. 2016, Science, 352, 1449
Mehringer, D. M., Palmer, P., Goss, W., & Yusef-Zadeh, F. 1993, ApJ, 412, 684
Motiyenko, R. A., Margulès, L., Goubet, M., et al. 2010, J. Phys. Chem. A, 114, 2794
Motiyenko, R. A., Margulès, L., Alekseev, E. A., & Guillemin, J.-C. 2015, J. Phys. Chem. A, 119, 1048
Neill, J. L., Muckle, M. T., Zaleski, D. P., et al. 2012, ApJ, 755, 153
Pickett, H. M. 1972, J. Chem. Phys., 56, 1715
Senent, M. 1998a, J. Mol. Spectr., 191, 265
Senent, M. 1998b, Chem. Phys. Lett., 296, 299
Senent, M. 2004, J. Phys. Chem. A, 108, 6286
Senent, M., Dalbouha, S., Cuisset, A., & Sadovskii, D. 2015, J. Phys. Chem. A, 119, 9644
Smirnov, I., Alekseev, E., Piddyachiy, V., Ilyushin, V., & Motiyenko, R. 2013, J. Mol. Spectr., 293, 33
Werner, H., Knowles, P., Knizia, G., et al. 2012, MOLPRO, version 2012.1, a package of ab initio programs, see http://www.molpro.net
Werner, H.-J., Adler, T. B., & Manby, F. R. 2007, J. Chem. Phys., 126, 164102
Woon, D. E. 2001, Icarus, 149, 277
Zakharenko, O., Motiyenko, R. A., Margulès, L., & Huet, T. R. 2015, J. Mol. Spectr., 317, 41